

X-RAY SPECTRAL PROPERTIES OF SEVEN HEAVILY OBSCURED SEYFERT 2 GALAXIES

S. MARCHESE¹, M. AJELLO¹, A. COMASTRI², G. CUSUMANO³, V. LA PAROLA³, A. SEGRETO³

Accepted for publication in the Astrophysical Journal on January 14, 2017

ABSTRACT

We present the combined *Chandra* and *Swift*-BAT spectral analysis of seven Seyfert 2 galaxies selected from the *Swift*-BAT 100-month catalog. We selected nearby ($z \leq 0.03$) sources lacking of a ROSAT counterpart and never previously observed with *Chandra* in the 0.3–10 keV energy range, and targeted these objects with 10 ks *Chandra* ACIS-S observations. The X-ray spectral fitting over the 0.3–150 keV energy range allows us to determine that all the objects are significantly obscured, having $N_{\text{H}} \geq 10^{23} \text{ cm}^{-2}$ at a >99% confidence level. Moreover, one to three sources are candidate Compton thick Active Galactic Nuclei (CT-AGN), i.e., have $N_{\text{H}} \geq 10^{24} \text{ cm}^{-2}$. We also test the recent “spectral curvature” method developed by Koss et al. (2016) to find candidate CT-AGN, finding a good agreement between our results and their predictions. Since the selection criteria we adopted have been effective in detecting highly obscured AGN, further observations of these and other Seyfert 2 galaxies selected from the *Swift*-BAT 100-month catalog will allow us to create a statistically significant sample of highly obscured AGN, therefore better understanding the physics of the obscuration processes.

Subject headings: galaxies: active — galaxies: nuclei — X-rays: galaxies

1. INTRODUCTION

The Cosmic X-ray Background (CXB), i.e., the difused X-ray emission observed in the energy range going from 1 to ~ 200 –300 keV, is mainly caused by unobscured and obscured Active Galactic Nuclei (AGN; e.g., Alexander et al. 2003; Gilli et al. 2007; Treister et al. 2009). However, while the unobscured AGN population, responsible for the CXB emission at < 10 keV, has been almost completely detected, at the present day only $\sim 30\%$ of the CXB at its peak (~ 30 keV, Ajello et al. 2008) has been directly detected, thanks to several surveys with the *NuSTAR* telescope (Aird et al. 2015; Civano et al. 2015; Harrison et al. 2015; Mullaney et al. 2015). Moreover, while theoretically Compton thick (CT-) AGN, i.e., sources with absorbing column density $N_{\text{H}} \geq 10^{24} \text{ cm}^{-2}$, are expected to be numerous (see, e.g., Risaliti et al. 1999) and responsible for ~ 10 –25% of the CXB emission at its peak, the fraction of CT-AGN detected with respect to the total number of AGN is so far $\sim 5\%$ (Comastri 2004; Della Ceca et al. 2008).

For AGN with column densities $\leq 10^{25} \text{ cm}^{-2}$, a fraction of direct nuclear emission can be observed at ≥ 10 keV; for larger column densities, instead, the only observable component in the same energy range is the scattered, indirect one (see, e.g., Matt et al. 1999; Yaqoob et al. 2010). Consequently, a complete census of the CT-AGN population requires deep observations above 10 keV. Burlon et al. (2011) analyzed the 15–55 keV spectral properties of a complete sample of AGN at $z < 0.1$ detected by *Swift*-BAT, founding that the observed fraction of CT-AGN in this sample is $\sim 5\%$. However, in the same work it was pointed out that even above 10 keV the AGN emission is strongly suppressed by absorption and Comp-

ton scattering. Therefore, the $\sim 5\%$ fraction of obscured AGN observed in most works in literature could not be intrinsic, but could actually being related to an observational bias. In fact, the modelling of this selection effect in Burlon et al. (2011) suggests that the intrinsic CT-AGN population accounts for about 20% of the whole AGN population. A similar intrinsic fraction of Compton thick sources has been computed also by Brightman & Nandra (2011) and Vasudevan et al. (2013).

While detecting CT-AGN remains a challenging task, in the last ten years several works were able to detect at least a part of these extremely obscured objects. Since at $z > 1$ the > 10 keV energy range is observable in the 0.5–10 keV band, deep-field surveys with *Chandra* and *XMM-Newton* have been able to detect CT-AGN at $z > 1$ (see, e.g., Georgantopoulos et al. 2013; Vignali et al. 2014; Buchner et al. 2015; Lanzuisi et al. 2015). A further step in detecting and analyzing candidate CT-AGN was the launch of *NuSTAR*, which allowed to study single sources with unprecedented statistics in the 5–50 keV band (see, e.g., Arévalo et al. 2014; Baloković et al. 2014; Gandhi et al. 2014; Annuar et al. 2015; Bauer et al. 2015; Koss et al. 2015; Lansbury et al. 2015; Boorman et al. 2016; Puccetti et al. 2016; Ricci et al. 2016).

AGN obscuration is usually linked to the presence of a so-called “dusty torus”, i.e., the gas and dust material surrounding the AGN accretion disk and responsible for the obscuration. This material is not continuously distributed, but more likely a clumpy distribution of optically thick dusty clouds (e.g., Elitzur & Shlosman 2006; Risaliti et al. 2007; Hönig & Beckert 2007; Nenkova et al. 2008). In the disk outflow scenario (Emmering et al. 1992) the obscuration is caused by a clumpy disk wind and can be described using two main parameters: the AGN luminosity and Eddington ratio. This model predicts that in the low-luminosity regime (i.e., at bolometric luminosities $L_{\text{bol}} \leq 10^{42} \text{ erg s}^{-1}$) the cloud outflow process cannot be sustained by the AGN and the broad line region (BLR) and the dusty clouds should both dis-

¹ Department of Physics & Astronomy, Clemson University, Clemson, SC 29634, USA

² INAF-Osservatorio Astronomico di Bologna, via Ranzani 1, 40127 Bologna, Italy

³ INAF - Istituto di Astrofisica Spaziale e Fisica Cosmica, Via U. La Malfa 153, I-90146 Palermo, Italy

appear (Nicastro 2000; Elitzur & Ho 2009). This prediction was observationally confirmed by Burlon et al. (2011), which found a decrease in the fraction of obscured AGN detected by *Swift*-BAT at $L_{15-55\text{ keV}} \leq 10^{43} \text{ erg s}^{-1}$. A similar behaviour may be linked to a change in the AGN accretion regime, switching from an optically thick, geometrically thin disk (e.g. Shakura & Sunyaev 1973) to a radiatively inefficient accretion flow (e.g., Narayan & Yi 1994; Blandford & Begelman 1999). However, a recent work by Brightman et al. (2015) did not find evidence of decrease of the obscured AGN fraction at low luminosities. Consequently, the detection and study of low-luminosity, highly obscured AGN becomes strategic to better understand the physics of the torus and the accretion disk.

In this work, we analyze the 0.3-150 keV spectra of seven nearby Seyfert 2 galaxies detected with *Swift*-BAT in the 15–150 keV band and reported in the *Swift*-BAT 100-month catalog. These sources have $L_{15-55\text{ keV}} \leq 10^{43} \text{ erg s}^{-1}$. We obtained a 10 ks follow-up with *Chandra* ACIS-S in the 0.3–7 keV band for each object in the sample. The combination of *Chandra* and *Swift*-BAT observations provides us an ideal dataset to properly characterize the main physical features of these sources, which are all expected to be heavily obscured and even Compton thick. In Section 2 we describe our sample and the data reduction procedure adopted for the *Chandra* data. In Section 3 we present the result of the spectral fitting procedure, a physical analysis of the best-fit models and a comparison with previous results for two of the seven sources. Finally, in Section 4 we discuss our results, focusing on the effectiveness of our selection procedure in detecting highly obscured AGN.

Throughout this work, we adopt a cosmology with $\Omega_m = 0.27$, $\Omega_\Lambda = 0.73$, and $H_0 = 71 \text{ km s}^{-1} \text{ Mpc}^{-1}$. Errors are quoted at 90% confidence level unless otherwise stated.

2. SAMPLE PROPERTIES AND DATA REDUCTION

The *Swift* satellite (Gehrels et al. 2004) is equipped with the wide-field ($120 \times 90 \text{ deg}^2$) Burst Alert Telescope (BAT; Barthelmy et al. 2005). This telescope performs imaging in the 15-150 keV energy range and has been continuously observing the whole sky since its launch. The most recent catalog of sources detected in the BAT survey data is the 100-month catalog⁴, which contains sources detected down to a flux limit $f \sim 3.3 \times 10^{-12} \text{ erg s}^{-1} \text{ cm}^{-2}$ in the 15-150 keV band. With its combination of good sensitivity and all-sky coverage, this instrument provides an excellent view of the hard X-ray low luminosity population in the nearby Universe. We point out that the 100-month BAT catalog is yet to be published (Segreto et al. in prep.), but all the data used in this work have been fully reprocessed.

To reprocess the BAT survey 100-month data available in the HEASARC public archive we used the BAT-IMAGER code (Segreto et al. 2010). This software has been developed to analyze data from coded mask instruments and performs screening, mosaicking and source detection. The spectra used in this work are background subtracted and have been obtained averaging over the whole BAT exposure. We used the official

BAT spectral redistribution matrix⁵.

In Table 1 we report the list of sources we analyze in this work. We selected from the *Swift*-BAT 100-month catalog seven nearby AGN ($z < 0.03$), associated to Seyfert 2 galaxies, lacking of a ROSAT counterpart in the 0.1–2.4 keV band. Two out of seven sources (ESO 116-G018 and NGC 5972) have never been observed before at 0.3–10 keV energies, and none of them has been previously observed using *Chandra*. The nearest source has $z=0.0122$ (i.e., $d \sim 52 \text{ Mpc}$), while the farthest has $z=0.0297$ ($d \sim 130 \text{ Mpc}$). The 15–55 keV luminosity range spans from $L_{\text{BAT}} \sim 2 \times 10^{42} \text{ erg s}^{-1}$ to $L_{\text{BAT}} \sim 2 \times 10^{43} \text{ erg s}^{-1}$. We selected low-redshift sources because the vast majority (>85%) of *Swift*-BAT-detected CT-AGN have so far been discovered at $z < 0.04$ (see, e.g., Burlon et al. 2011; Ricci et al. 2015). Moreover, the lacking of a ROSAT counterpart is already a hint of at least moderate obscuration, with $N_{\text{H}} \gtrsim 10^{22} \text{ cm}^{-2}$ (see, e.g., Figure 2 of Koss et al. 2016).

All the sources have been targeted with 10 ks *Chandra* ACIS-S observations during *Chandra* Cycle 17 (Proposal number 17900432, P.I. Marco Ajello). The data have been reduced with the CIAO (Fruscione et al. 2006) 4.7 software and the *Chandra* Calibration Data Base (caldb) 4.6.9, adopting standard procedures; no source shows significant pile-up, as measured by the CIAO PILEUP_MAP tool. Source and background spectra have been extracted using the CIAO *specextract* tool. Source spectra have been extracted in circular regions of $4''$, while background have been extracted from annuli having internal radius $r_{\text{int}}=7''$ and external radius $r_{\text{out}}=20''$, after a visual inspection to avoid contamination from nearby sources. Point-source aperture correction was applied during the source spectral extraction process. Finally, the spectra were binned in order to have at least 15 bins in the *Chandra* spectrum: each bin contains from 8 to 20 counts, according to the source brightness.

3. SPECTRAL FITTING RESULTS

In Table 2 we report the results of the spectral fitting of the seven *Swift*-BAT Seyfert 2 galaxies in our sample. The spectral fitting has been performed using XSPEC v. 12.9.0 (Arnaud 1996). Galactic absorption was determined using the Heasoft tool *nh* (Kalberla et al. 2005).

All sources have first been fitted with a basic power law with photon index Γ and intrinsic absorption $N_{\text{H},z}$ caused by the dusty torus surrounding the AGN accretion disk. The intrinsic absorption is computed using the MyTorus model (Murphy & Yaqoob 2009), which assumes a toroidal distribution of the absorbing material and is particularly effective in fitting spectra of heavily obscured objects.

We determined that for all seven sources in the sample more complex models than the basic absorbed power law one were required to significantly improve the fit. The significance of the additional components has been verified performing a F-test, when statistically allowed; in the remaining cases (i.e., when a Gaussian or a reflection component were added, see Protassov et al. 2002) the fits without the additional components always had reduced χ^2 , $\chi^2/(\text{degrees of freedom}) > 1.5$, while the best-fit with

⁴ http://bat.ifa.inaf.it/100m_bat_catalog/100m_bat_catalog_v0.0.htm

⁵ <http://heasarc.gsfc.nasa.gov/docs/heasarc/caldb/data/swift/bat/index.html>

<i>Swift</i> -BAT ID	Source name	R.A. deg (J2000)	Dec deg (J2000)	z	$L_{15-55\text{ keV}}$ erg s $^{-1}$	Obs ID	Obs Date
J1253.5-4844	NGC 4785	193.3639	-48.7492	0.0123	2.3×10^{42}	18074	2016 Apr 16
J1024.6-2332	ESO 500-G034	156.1310	-23.5530	0.0122	1.8×10^{42}	18075	2016 Feb 08
J0333.7-0504	NGC 1358	53.4153	-5.0894	0.0134	2.0×10^{42}	18076	2015 Nov 21
J0324.8-6043	ESO 116-G018	51.2210	-60.7384	0.0185	2.5×10^{42}	18077	2016 Aug 05
J0448.9-5739	ESO 119-G008	72.2364	-57.6592	0.0229	4.4×10^{42}	18078	2016 Jul 09
J2234.9-2543	ESO 533-G050	338.7076	-25.6769	0.0264	1.1×10^{43}	18079	2016 May 22
J1539.0+1701	NGC 5972	234.7257	17.0262	0.0297	1.0×10^{43}	18080	2016 Apr 04

Table 1

Summary of the sources in our sample. All the *Swift*-BAT IDs come from the Palermo BAT Catalog fourth version (4PBC). “Obs ID” and “Obs Date” refer to the *Chandra* observations.

the additional component has reduced $\chi^2 \sim 1$.

These are the different components we used in the fit, in addition to the basic absorbed power law. The best-fit models for each source are reported in Table 2.

1. Six spectra require a second power law component, having photon index $\Gamma_2 = \Gamma_1$, the photon index of the main power law, and not affected by the intrinsic absorption $N_{\text{H},z}$. This second power law accounts for a fraction of AGN emission unabsorbed by the torus and/or for a scattered component, i.e., light deflected rather than absorbed by the dust and gas. The normalization of this second component is always $< 1\%$ than the normalization of the main power law.
2. Four fits are significantly improved adding the *MyTorus* fluorescent emission line component to model an excess in the spectrum at energy $E \sim 6.4$ keV. The line in the model was fixed at 6.4 keV (rest-frame) and accounts for the presence of the iron $K\alpha$ line. The iron $K\alpha$ equivalent width varies in the range $\text{EW} = [0.15-0.75]$ keV (we report the EW values in Table 2).
3. Two sources in the sample require the addition of a black body component with $kT < 0.3$ keV to model the characteristic “soft excess” commonly observed in the AGN spectra and possibly due to the presence of warm gas close to the AGN accretion disk or in the BLR (see, e.g., Risaliti & Elvis 2004). In order to understand the origin of this excess, for these two sources (NGC 1358 and NGC 5972) we used the equations reported in Lehmer et al. (2010) to quantify the expected contribution of star-forming (SF) processes to the X-ray emission. We used the IRAS 8–1000 μm luminosities to compute the star-formation rate (SFR) and SFR to estimate $L_{2-10\text{ keV}}^{\text{SF}}$. For both sources, we find $L_{2-10\text{ keV}}^{\text{SF}} \leq 10^{39}$ erg s $^{-1}$, i.e., $\lesssim 0.1\%$ of the AGN luminosity in the energy range, therefore safely ruling out a significant SF contribution to the X-ray emission.
4. One source in the sample (NGC 5972) shows an excess in the *Swift*-BAT spectrum at $E \sim 30$ keV which is best-fitted with the *PEXRAV* model (Magdziarz & Zdziarski 1995), which parametrizes a power law with a significant reflection component. This reflection component is caused by cold material surrounding the accretion disk. Due to the low statis-

tics of the spectrum of NGC 5972, we fixed the reflection scaling factor R to 1. Since it is $R = \Omega/2\pi$, where Ω is the solid angle of the cold material, responsible for the reflection, visible from the hot corona, responsible from the X-ray emission, $R=1$ is the case where the reflection is produced by an infinite slab isotropically illuminated by the corona emission.

Since the *Swift*-BAT spectrum is averaged on 100 months of observations, while the *Chandra* one is obtained by a single observation, the joint fit of the *Chandra* and *Swift*-BAT spectra requires the addition of a multiplicative constant (C_{BAT}) to the *Swift*-BAT spectrum, to account for both flux variability and cross-correlation offsets. We examined the *Swift*-BAT light curves of the seven sources in our sample and none of them shows strong flares, the flux variability being limited to 20–40%. For five out of seven sources, the best-fit constant we obtained is consistent (within the errors) to $C_{\text{BAT}}=1$ and can be explained with the variability observed in the *Swift*-BAT light curves. For two AGN (NGC 1358 and ESO 116-G018), however, the best-fit constant we find is significantly higher, being ~ 9 and ~ 3 , respectively. Such a high variability cannot be ruled out on the basis of our observations, since NGC 1358 and/or ESO 116-G018 could be changing-look AGN (i.e., sources with a significant change in flux and/or amount of obscuring material); however, similar flux variations are extremely unlikely in highly obscured sources, the reflection component washing out fluctuations on short timescales (see, e.g., Gandhi et al. 2015). Therefore, for these two sources we fixed C_{BAT} to 1.

In Figure 1 we show the $N_{\text{H},z}$ distribution versus redshift for the sources in our sample, while in Figures 2 and 3 we report the seven spectra and their best fits. In the inset, we also report the confidence contours for Γ and $N_{\text{H},z}$: as can be seen, all the sources are heavily obscured. We will discuss in detail the $N_{\text{H},z}$ measurements in the next section: here we point out that, as a consequence of the heavy obscuration, which affects mainly the 0.3–7 keV band, the ratio between the flux in the 15–150 keV band and the flux in the 0.3–7 keV one is > 10 for all the sources in our sample and even > 30 for the three most obscured objects.

3.1. Intrinsic absorption and its trend with torus inclination angle

One of the *MyTorus* model parameters is θ , the inclination angle between the observer line of sight and the

<i>Swift</i> -BAT ID	$N_{\text{H,gal}}$ 10^{20} cm^{-2}	$N_{\text{H,z},\theta=90}$ 10^{22} cm^{-2}	$N_{\text{H,z},\theta=65}$ 10^{22} cm^{-2}	θ_{max} °	Γ	EW keV	kT_{BB} keV	SC	χ^2/DOF	Model
NGC 4785	12.2	$41.38^{+10.94}_{-8.75}$	$77.37^{+20.65}_{-16.47}$	–	$1.86^{+0.21}_{-0.19}$	$0.48^{+0.33}_{-0.34}$	–	0.47 ± 0.13	7.9/15	po+MyT*(po+zga)
ESO 500-G034	5.1	$57.41^{+13.48}_{-10.80}$	$107.60^{+25.26}_{-20.24}$	66	$2.30^{+0.27}_{-0.24}$	–	–	0.18 ± 0.06	12.3/15	po+MyT*po
NGC 1358	3.8	$104.87^{+42.14}_{-35.80}$	$196.44^{+211.09}_{-67.03}$	90	$1.59^{+0.46}_{-0.45}$	$0.75^{+0.75}_{-0.74}$	$0.16^{+0.12}_{-0.11}$	0.77 ± 0.42	14.8/13	po+MyT*(bb+po+zga)
ESO 116-G018	3.1	$94.68^{+46.06}_{-39.97}$	$178.13^{+86.19}_{-75.34}$	81	$1.86^{+0.51}_{-0.48}$	$1.41^{+2.67}_{-0.94}$	–	0.52 ± 0.29	17.2/14	po+MyT*(po+zga)
ESO 119-G008	1.3	$18.15^{+6.18}_{-5.49}$	$34.02^{+11.57}_{-10.28}$	–	$1.77^{+0.21}_{-0.18}$	–	–	0.39 ± 0.10	17.7/20	po+MyT*po
ESO 533-G050	1.5	$22.56^{+5.45}_{-4.74}$	$42.24^{+10.23}_{-8.88}$	–	$1.65^{+0.18}_{-0.14}$	$0.15^{+0.17}_{-0.15}$	–	0.54 ± 0.12	25.6/22	MyT*(po+zga)
NGC 5972	3.0	$78.62^{+16.94}_{-12.34}$	$147.27^{+79.89}_{-59.22}$	72	$1.63^{+0.23}_{-0.09}$	–	$0.14^{+0.07}_{-0.05}$	0.65 ± 0.35	17.6/16	po+MyT*(bb+pexr)

Table 2

Best fit properties for the seven Seyfert 2 galaxies in our sample. The XSPEC components reported in the “model” columns are the following: **pow** is a power law with photon index Γ ; when two power laws are present, their photon index is the same. **zga** is the MyTorus Iron $K\alpha$ component with equivalent width EW. **bb** is a black-body component having temperature kT_{BB} and fitting a soft excess observed below 1 keV. **pexr** is a power law with a cold matter reflection component. The intrinsic absorption $N_{\text{H,z}}$ is modeled with MyTorus (MyT in the table), with inclination angle θ equal to 65° or to 90° . θ_{max} is the maximum inclination angle for which is $N_{\text{H,z}} > 10^{24} \text{ cm}^{-2}$. SC is the spectral curvature value computed following Koss et al. (2016)

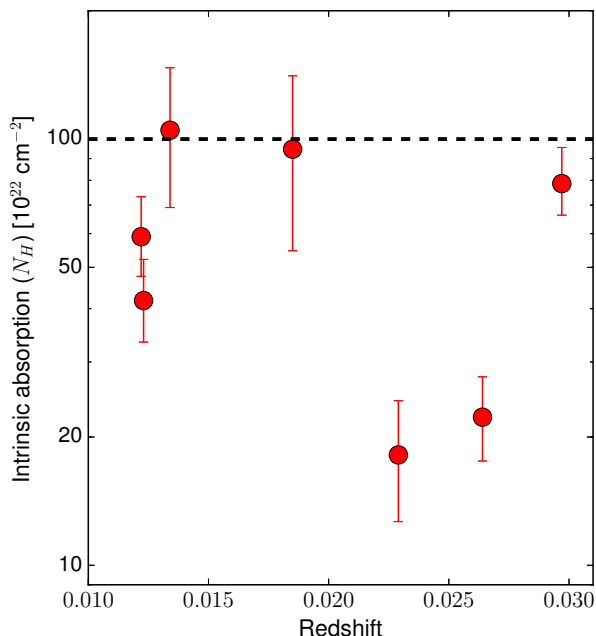


Figure 1. Intrinsic absorption $N_{\text{H,z}}$, computed assuming $\theta=90^\circ$, as a function of redshift, for the seven sources in our sample. The horizontal dashed line marks the Compton-thick regime, i.e., $N_{\text{H,z}} \geq 10^{24} \text{ cm}^{-2}$.

torus symmetry axis, with $\theta=0^\circ$ being a face-on observing angle and $\theta=90^\circ$ being an edge-on observing angle. $\theta=60^\circ$ is the torus opening angle, while $\theta=61^\circ$ is the lowest angle for which the observer line of sight intercepts the torus.

The quality of our spectra does not allow us to constrain $N_{\text{H,z}}$ and θ simultaneously. Therefore, we fitted our data twice: the first one assuming $\theta=90^\circ$, i.e., the edge-on scenario, the second one with $\theta=65^\circ$, i.e., an angle closer to the angle for which the observer line of sight intercepts the torus. As can be seen in Table 2, assuming $\theta=65^\circ$ implies obtaining best-fit $N_{\text{H,z}}$ values ~ 2 times higher than those obtained assuming $\theta=90^\circ$.

As already pointed out in the previous section, all

sources in our sample are heavily obscured. Even in the worst case scenario, i.e., assuming that all sources are observed edge-on, ($\theta=90^\circ$), all the objects have $N_{\text{H,z}} > 10^{23} \text{ cm}^{-2}$ at a 99% confidence level. Moreover, four out of seven sources can in principle be CT-AGN, assuming that we are observing them with a θ close to the torus opening angle: in such a scenario, the path of the photons across the torus and the intrinsic absorption value are respectively smaller and larger than in the case with $\theta=90^\circ$.

To complete our analysis, we re-fitted the spectra with two other models to describe the absorbed power-law: the first one is the standard photo-electric absorption (**zfabs** in XSpec), while the other is **pclabs**, which describes the X-ray emission of an isotropic source of photons, corrected by the absorption caused by a spherical distribution of material. In this second model, Compton scattering is taken into account. In both cases, we find that the $N_{\text{H,z}}$ best-fit values are consistent (within the errors) with the MyTorus best-fit values obtained assuming $\theta=90^\circ$. These results may indicate that reliable θ values are closer to the $\theta=90^\circ$ limit than to the $\theta=65^\circ$ one. However, a proper disentanglement of the $N_{\text{H,z}}-\theta$ can be broken only increasing the 0.3–7 keV band exposure (see Section 4 for further details).

3.2. Comparison with previous results

Two sources in our sample have already been observed in the 0.5–10 keV band. In this section, we present previously published works and we compare their results with ours.

NGC 1358 was targeted with a 10 ks XMM-Newton observation in 2005 (PI: I. Georgantopoulos): the spectral fitting results for this observation (the *Swift*-BAT spectrum was not used in this work) have been published in Marinucci et al. (2012). Their results are in good agreement with ours: they find that NGC 1358 is consistent with being a CT-AGN, although with large uncertainties, having best-fit intrinsic absorption $N_{\text{H,z}} = 1.3^{+8.5}_{-0.6} \times 10^{24} \text{ cm}^{-2}$.

NGC 4785 has already been studied by Gandhi et al. (2015): they combined the *Swift*-BAT observation used in this work with a 79 ks *Suzaku* observation. They fitted the data with PEXRAV, with MyTorus and with the

TORUS model by Brightman & Nandra (2011). In all cases, they found the source being Compton-thick, the measured intrinsic absorption varying from $N_{\text{H},z}=1.4_{-0.9}^{+0.5}$ cm^{-2} while fitting the data with PEXRAV to $N_{\text{H},z}=2.7_{-0.8}^{+3.8}$ cm^{-2} fitting the data with TORUS. Our $N_{\text{H},z}$ estimate is therefore consistent, within the errors, with their PEXRAV best-fit, and lie below their results with MyTorus and TORUS. While the hypothesis that this discrepancy can be partially driven by the low statistics in our fit, which has only 16 degrees of freedom, compared to the 89 of the Gandhi et al. (2015) one, it is also possible that the change in the measure intrinsic absorption is due to intrinsic variability in the amount of obscuring material in the time between the *Suzaku* observation (taken in July 2013) and the *Chandra* one (taken in April 2016). A significant change of the AGN luminosity seems less likely, since the power-law photon index we measured ($\Gamma=1.80_{-0.19}^{+0.21}$) is in good agreement with the one of Gandhi et al. (2015) ($\Gamma=2.1_{-0.3}^{+0.4}$ using MyTorus). Finally, Gandhi et al. (2015) find evidence of a strong Iron $K\alpha$ line in NGC 4785, with $\text{EW}=1.1_{-0.4}^{+u}$ keV (where u means unconstrained), while the EW of the line in our fit is weaker ($\text{EW}=0.48_{-0.34}^{+0.33}$). This change in line intensity may strengthen the hypothesis that we are observing a variation in the amount of obscuring material, since CT-AGN usually show prominent iron lines with $\text{EW}>1$ keV (see, e.g., Koss et al. 2016).

4. DISCUSSION AND CONCLUSIONS

In this work, we presented the spectral fitting over the 0.3–150 keV energy range, obtained combining *Chandra* and *Swift*-BAT observations, of seven AGN at $z < 0.03$ selected from the 100-month *Swift*-BAT all-sky survey catalog. These sources are associated to Seyfert 2 galaxies and lack of a ROSAT counterpart in the 0.1–2.4 keV band. The combined *Chandra* and *Swift*-BAT spectra have then been fitted with different models, to estimate spectral parameters such as the spectral photon index Γ and the intrinsic absorption $N_{\text{H},z}$.

As discussed in Section 3.1, all the sources in the sample are heavily obscured: even in the (unlikely) scenario of all the sources being edge-on (i.e., with inclination angle $\theta=90^\circ$) the less obscured object (ESO 119-G008) has $N_{\text{H},z}=1.82_{-0.55}^{+0.62} \times 10^{23}$ cm^{-2} and all sources have $N_{\text{H},z} > 10^{23}$ cm^{-2} at a 99% confidence level. Moreover, one source (NGC 1358) has best-fit intrinsic absorption $N_{\text{H},z}=1.05_{-0.36}^{+0.42} \times 10^{24}$ cm^{-2} , i.e., consistent with being a Compton thick AGN.

Furthermore, we performed a further fitting analysis varying θ in 1° steps, and we found that five of the sources in our sample can be CT-AGN, if the inclination angle θ between the observer line of sight and the torus rotation axis is small enough (see column θ_{max} in Table 2).

A first important result of this work is therefore the finding of an effective way to detect obscured AGN in the nearby Universe, taking advantage of the combination of low limiting flux and wide field of view of the *Swift*-BAT all-sky survey. It is worth noticing that, while with our selection technique we detect a population of sources with $N_{\text{H},z} > 10^{23}$ cm^{-2} , the observed fraction of unobscured AGN (i.e., with $N_{\text{H},z} < 10^{22}$ cm^{-2}) ob-

tained without applying any selection criteria is 35–55% (Burlon et al. 2011).

Koss et al. (2016) developed a technique to identify CT-AGN in AGN with low counts statistics observed with *Swift*-BAT or *NuSTAR*, finding that the fraction of CT-AGN at $z < 0.03$ is $\sim 22\%$. The Koss et al. (2016) method is based on the curvature of the AGN spectrum between 14 and 50 keV, parametrized as follows:

$$SC_{\text{BAT}} = \frac{-3.42A - 0.82B + 1.65C + 3.58D}{\text{Tot}}, \quad (1)$$

where A , B , C , D and Tot are the count rates measured with *Swift*-BAT in the 14–20 keV, 20–24 keV, 24–35 keV, 35–50 keV and 14–50 keV, respectively. $SC_{\text{BAT}}=0.4$ is the CT-AGN selection threshold: in Koss et al. (2016) work, seven of the nine sources with $SC_{\text{BAT}} > 0.4$ in their sample have $N_{\text{H},z} > 10^{24}$ cm^{-2} , and the remaining two are significantly obscured ($N_{\text{H},z} > 5 \times 10^{23}$ cm^{-2}).

In Table 2 we report the SC_{BAT} values for the seven sources in our sample: as can be seen, the Koss et al. (2016) assumption on SC_{BAT} is supported by our results. In fact, the most obscured source in our sample (NGC 1358) has $SC_{\text{BAT}}=0.77 \pm 0.42$, i.e., the highest SC_{BAT} value for the sources in our sample, although the uncertainty on the SC value is quite large. Other two highly obscured sources (ESO 116-G018 and NGC 5972), both have $SC_{\text{BAT}} > 0.4$ ($SC_{\text{BAT}}=0.52 \pm 0.29$ and $SC_{\text{BAT}}=0.65 \pm 0.35$, respectively), although both the sources have $SC_{\text{BAT}} < 0.4$ at a 90% confidence level. These two objects have $N_{\text{H},z} < 10^{24}$ cm^{-2} assuming $\theta=90^\circ$, but may have $N_{\text{H},z} > 10^{24}$ cm^{-2} assuming reasonable values of θ (81° and 72° , respectively). Finally, two sources with $SC_{\text{BAT}} > 0.4$, and therefore candidate CT-AGN according to the Koss et al. (2016) equation, have $N_{\text{H},z} \sim 2\text{--}4 \times 10^{23}$ cm^{-2} assuming $\theta=90^\circ$.

The results of this work represent a first step in the process of identifying and analyzing CT-AGN in the local Universe. To improve our findings, we plan to extend our analysis in two ways:

1. Increasing the exposure for the objects we described in this work, using *XMM-Newton*, *Chandra* and *NuSTAR*. The 0.3–7 keV spectra studied in this work have been obtained with observations of only 10 ks each, and have between 80 (for the two most obscured AGN in our sample) and 270 (ESO 533-G050) net counts in the 0.3–7 keV band: breaking the degeneracy between the intrinsic absorption $N_{\text{H},z}$ and the inclination angle θ , therefore definitely assessing if a source is or is not a CT-AGN, requires a larger counts statistics. As a comparison, Tanimoto et al. (2016) constrained simultaneously $N_{\text{H},z}$ and θ for the three candidate CT-AGN observed with *Suzaku* for 30–70 ks and having each about 500 net counts in the 0.3–7 keV band.
2. Increasing the sample of candidate CT-AGN. The selection criteria we adopted in this work proved very effective, and the *Swift*-BAT 100-month catalog contains other $\sim 5\text{--}10$ sources at $z < 0.04$ that are Seyfert 2 galaxies lacking of ROSAT counterpart and which have not been observed by either

Chandra or *XMM-Newton*. We plan to target these sources with future *Chandra* and *XMM-Newton* observations.

REFERENCES

- Aird, J., Alexander, D. M., Ballantyne, D. R., et al. 2015, *ApJ*, 815, 66
- Ajello, M., Greiner, J., Sato, G., et al. 2008, *ApJ*, 689, 666
- Alexander, D. M., Bauer, F. E., Brandt, W. N., et al. 2003, *AJ*, 126, 539
- Annuar, A., Gandhi, P., Alexander, D. M., et al. 2015, *ApJ*, 815, 36
- Arévalo, P., Bauer, F. E., Puccetti, S., et al. 2014, *ApJ*, 791, 81
- Arnaud, K. A. 1996, in *Astronomical Society of the Pacific Conference Series*, Vol. 101, *Astronomical Data Analysis Software and Systems V*, ed. G. H. Jacoby & J. Barnes, 17
- Baloković, M., Comastri, A., Harrison, F. A., et al. 2014, *ApJ*, 794, 111
- Barthelmy, S. D., Barbier, L. M., Cummings, J. R., et al. 2005, *Space Sci. Rev.*, 120, 143
- Bauer, F. E., Arévalo, P., Walton, D. J., et al. 2015, *ApJ*, 812, 116
- Blandford, R. D. & Begelman, M. C. 1999, *MNRAS*, 303, L1
- Boorman, P. G., Gandhi, P., Alexander, D., et al. 2016, *ArXiv e-prints* [1610.08997]
- Brightman, M., Baloković, M., Stern, D., et al. 2015, *ApJ*, 805, 41
- Brightman, M. & Nandra, K. 2011, *MNRAS*, 413, 1206
- Buchner, J., Georgakakis, A., Nandra, K., et al. 2015, *ApJ*, 802, 89
- Burlon, D., Ajello, M., Greiner, J., et al. 2011, *ApJ*, 728, 58
- Civano, F., Hickox, R. C., Puccetti, S., et al. 2015, *ApJ*, 808, 185
- Comastri, A. 2004, in *Astrophysics and Space Science Library*, Vol. 308, *Supermassive Black Holes in the Distant Universe*, ed. A. J. Barger, 245
- Della Ceca, R., Caccianiga, A., Severgnini, P., et al. 2008, *A&A*, 487, 119
- Elitzur, M. & Ho, L. C. 2009, *ApJL*, 701, L91
- Elitzur, M. & Shlosman, I. 2006, *ApJL*, 648, L101
- Emmering, R. T., Blandford, R. D., & Shlosman, I. 1992, *ApJ*, 385, 460
- Fruscione, A., McDowell, J. C., Allen, G. E., et al. 2006, in *Proc. SPIE*, Vol. 6270, *Society of Photo-Optical Instrumentation Engineers (SPIE) Conference Series*, 62701V
- Gandhi, P., Lansbury, G. B., Alexander, D. M., et al. 2014, *ApJ*, 792, 117
- Gandhi, P., Yamada, S., Ricci, C., et al. 2015, *MNRAS*, 449, 1845
- Gehrels, N., Chincarini, G., Giommi, P., et al. 2004, *ApJ*, 611, 1005
- Georgantopoulos, I., Comastri, A., Vignali, C., et al. 2013, *A&A*, 555, A43
- Gilli, R., Comastri, A., & Hasinger, G. 2007, *A&A*, 463, 79
- Harrison, F. A., Aird, J., Civano, F., et al. 2015, *ArXiv e-prints* [1511.04183]
- Hönig, S. F. & Beckert, T. 2007, *MNRAS*, 380, 1172
- Kalberla, P. M. W., Burton, W. B., Hartmann, D., et al. 2005, *A&A*, 440, 775
- Koss, M. J., Assef, R., Baloković, M., et al. 2016, *ApJ*, 825, 85
- Koss, M. J., Romero-Cañizales, C., Baronchelli, L., et al. 2015, *ApJ*, 807, 149
- Lansbury, G. B., Gandhi, P., Alexander, D. M., et al. 2015, *ApJ*, 809, 115
- Lanzuisi, G., Ranalli, P., Georgantopoulos, I., et al. 2015, *A&A*, 573, A137
- Lehmer, B. D., Alexander, D. M., Bauer, F. E., et al. 2010, *ApJ*, 724, 559
- Magdziarz, P. & Zdziarski, A. A. 1995, *MNRAS*, 273, 837
- Marinucci, A., Bianchi, S., Nicastro, F., Matt, G., & Goulding, A. D. 2012, *ApJ*, 748, 130
- Matt, G., Pompilio, F., & La Franca, F. 1999, *NA*, 4, 191
- Mullaney, J. R., Del-Moro, A., Aird, J., et al. 2015, *ApJ*, 808, 184
- Murphy, K. D. & Yaqoob, T. 2009, *MNRAS*, 397, 1549
- Narayan, R. & Yi, I. 1994, *ApJL*, 428, L13
- Nenkova, M., Sirocky, M. M., Ivezić, Ž., & Elitzur, M. 2008, *ApJ*, 685, 147
- Nicastro, F. 2000, *ApJL*, 530, L65
- Protassov, R., van Dyk, D. A., Connors, A., Kashyap, V. L., & Siemiginowska, A. 2002, *ApJ*, 571, 545
- Puccetti, S., Comastri, A., Bauer, F. E., et al. 2016, *A&A*, 585, A157
- Ricci, C., Bauer, F. E., Treister, E., et al. 2016, *ApJ*, 819, 4
- Ricci, C., Ueda, Y., Koss, M. J., et al. 2015, *ApJL*, 815, L13
- Risaliti, G. & Elvis, M. 2004, in *Astrophysics and Space Science Library*, Vol. 308, *Supermassive Black Holes in the Distant Universe*, ed. A. J. Barger, 187
- Risaliti, G., Elvis, M., Fabbiano, G., et al. 2007, *ApJL*, 659, L111
- Risaliti, G., Maiolino, R., & Salvati, M. 1999, *ApJ*, 522, 157
- Segreto, A., Cusumano, G., Ferrigno, C., et al. 2010, *A&A*, 510, A47
- Shakura, N. I. & Sunyaev, R. A. 1973, *A&A*, 24, 337
- Tanimoto, A., Ueda, Y., Kawamuro, T., & Ricci, C. 2016, *PASJ*, 68, S26
- Treister, E., Urry, C. M., & Virani, S. 2009, *ApJ*, 696, 110
- Vasudevan, R. V., Brandt, W. N., Mushotzky, R. F., et al. 2013, *ApJ*, 763, 111
- Vignali, C., Mignoli, M., Gilli, R., et al. 2014, *A&A*, 571, A34
- Yaqoob, T., Murphy, K. D., Miller, L., & Turner, T. J. 2010, *MNRAS*, 401, 411

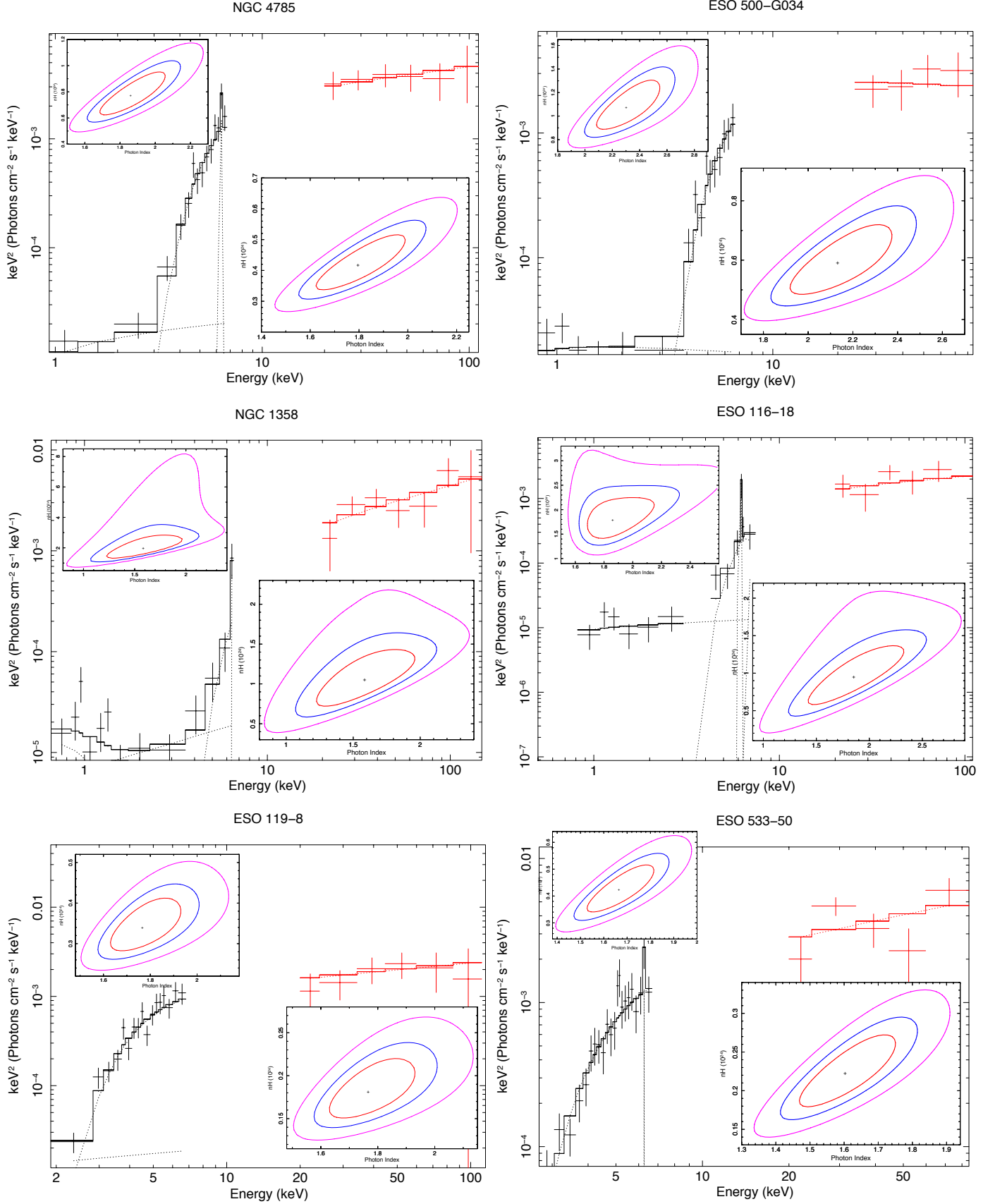


Figure 2. *Chandra* (black) and *Swift*-BAT (red) spectra of six of the seven sources in our sample. The best-fitting model is plotted as a solid line, while the single components are plotted as dotted lines. In the inset, the confidence contours at 68, 90 and 99% confidence level for Γ and $N_{\text{H,z}}$ (in units of 10^{24} cm^{-2}) are shown, assuming $\theta=90^\circ$ (bottom right) and $\theta=65^\circ$ (top left).

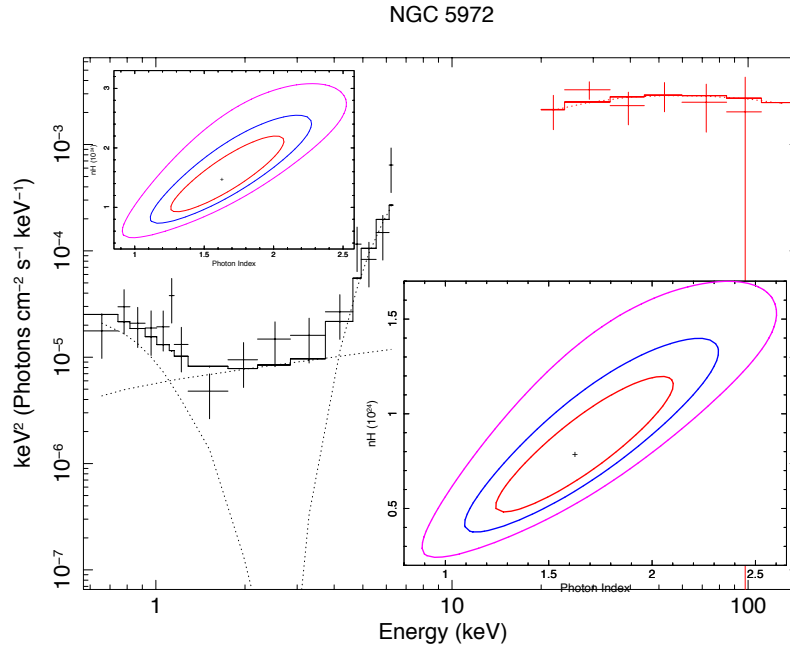


Figure 3. *Chandra* (black) and *Swift*-BAT (red) spectra of NGC 5972. The best-fitting model is plotted as a solid line, while the single components are plotted as dotted lines. In the inset, the confidence contours at 68, 90 and 99% confidence level for Γ and $N_{\text{H},z}$ (in units of 10^{24} cm^{-2}) are shown, assuming $\theta=90^\circ$ (bottom right) and $\theta=65^\circ$ (top left).